

Spectral Characterization for Small Clusters of Silicon and Oxygen: SiO, SiO₃, Si₂O₃, & Si₂O₄

Mason B. Gardner¹, Brent R. Westbrook¹, and Ryan C. Fortenberry²

¹University of Mississippi

²Unviersity of Mississippi

November 23, 2022

Abstract

Infrared spectra of evolved stars have a rise in signal between the 7.0 μm and 8.0 μm wavelengths; the antisymmetric Si-O stretches of small silicon oxide clusters fall in this range and have large intensities. Hence, this quantum chemical analysis provides data for such molecules that may be of significance for astrochemical classification and could play a role in the formation or degradation of mineral nanocrystals from or into their constituent atoms. Both explicitly computed anharmonic fundamental vibrational frequencies and those determined from scaled harmonic frequencies agree well with known experimental data, and spectroscopic constants are provided herein such that astronomical rotational spectral characterization may also be possible for the C₂v SiO₃ and Si₂O₃ molecules.

**Spectral Characterization for Small Clusters of Silicon
and Oxygen: SiO₂, SiO₃, Si₂O₃, & Si₂O₄**

Mason B. Gardner¹, Brent R. Westbrook¹, and Ryan C. Fortenberry¹

¹Department of Chemistry & Biochemistry, University of Mississippi, University, MS 38677-1848

Key Points:

- Small silicon oxide clusters have bands in detectable IR ranges.
- These may be intermediates between atoms and mineral nanocrystals.
- The spectral data produced here agree well with known experimental values and extend beyond it.

10 **Abstract**

11 Infrared spectra of evolved stars have a rise in signal between the $7.0\text{ }\mu\text{m}$ and $8.0\text{ }\mu\text{m}$
 12 wavelengths; the antisymmetric Si–O stretches of small silicon oxide clusters fall in
 13 this range and have large intensities. Hence, this quantum chemical analysis provides
 14 data for such molecules that may be of significance for astrochemical classification and
 15 could play a role in the formation or degradation of mineral nanocrystals from or into
 16 their constituent atoms. Both explicitly computed anharmonic fundamental vibrational
 17 frequencies and those determined from scaled harmonic frequencies agree well with known
 18 experimental data, and spectroscopic constants are provided herein such that astronomical
 19 rotational spectral characterization may also be possible for the C_{2v} SiO_3 and Si_2O_3
 20 molecules.

21 **Plain Language Summary**

22 Rocky bodies are made of minerals comprised largely of silicon and oxygen. How
 23 these minerals are formed from their constituent atoms is not fully known. The IR data
 24 produced in this work may help to observe small molecules containing silicon and oxy-
 25 gen so that these potential molecular intermediates can be observed. These molecules
 26 have strong absorption features between $7.0\text{ }\mu\text{m}$ and $8.0\text{ }\mu\text{m}$, most notably, and are now
 27 fully characterized in the IR.

28 **1 Introduction**

29 Quartz, sand, and silica are all forms for the most abundant material in the Earth's
 30 crust and mantle. Crystalline SiO_2 gives way to the molten form deeper into the man-
 31 tle, and it mixes with magnesium, iron, and aluminum to form most of the material present
 32 between the crust and core (White, 2013). Similar processes likely played out all over
 33 the early Solar System and even beyond since both oxygen and silicon are two of the most
 34 abundant atoms in the Universe (Savage & Sembach, 1996; McCall, 2006; Fortenberry,
 35 2020). Consequently, there are few inorganic materials as common as silicon dioxide.

36 Silicon dioxide boils at nearly 3300 K and becomes isovalent with carbon dioxide
 37 in its triatomic molecular form. Such would likely be a necessary signature of silicon-based
 38 metabolism in exobiology. With regards to less exotic applications, silicates are known
 39 to condense under cold conditions creating rocky material in the first place (Rouillé et
 40 al., 2014), and these small molecules likely aggregate from silicon and oxygen atoms or
 41 the SiO monomer which has been observed in astrophysical environments since 1971 (Wilson
 42 et al., 1971). At the other end of the star's lifetime, the ablation of rocky materials as
 43 a star dies (McCarthy et al., 2019) or the stellar infall of most solid materials at any stage
 44 in a star's evolution will likely vaporize the crystalline or even molten silicates and quartzes
 45 creating small silicon oxide molecules for which little spectral data are well-known. A
 46 similar vaporization process would also take place terrestrially in foundries when high
 47 temperatures are utilized in large-scale industrial processes. Regardless of the circum-
 48 stance, further spectral analysis of small silicon oxide clusters in the gas phase is nec-
 49 essary to produce data for the classification of silicon dioxide and its derivatives (Wang
 50 et al., 1997) such that the evolution of silicate materials from atoms to solids can be ob-
 51 served geophysically or industrially.

52 Argon matrix experiments have provided vibrational frequencies for the antisym-
 53 metric stretch and bending fundamentals of isolated SiO_2 at 1416 cm^{-1} and 273 cm^{-1} ,
 54 respectively (H. Schnöckel, 1978; V. H. Schnöckel, 1980; Andrews & McCluskey, 1992;
 55 Jacox, 1994). Five of the six fundamental frequencies of SiO_3 have been tentatively as-
 56 signed from similar experiments in conjunction with density functional theory analysis
 57 (DFT) (Tremblay et al., 1996), but follow-up work has not conclusively confirmed such

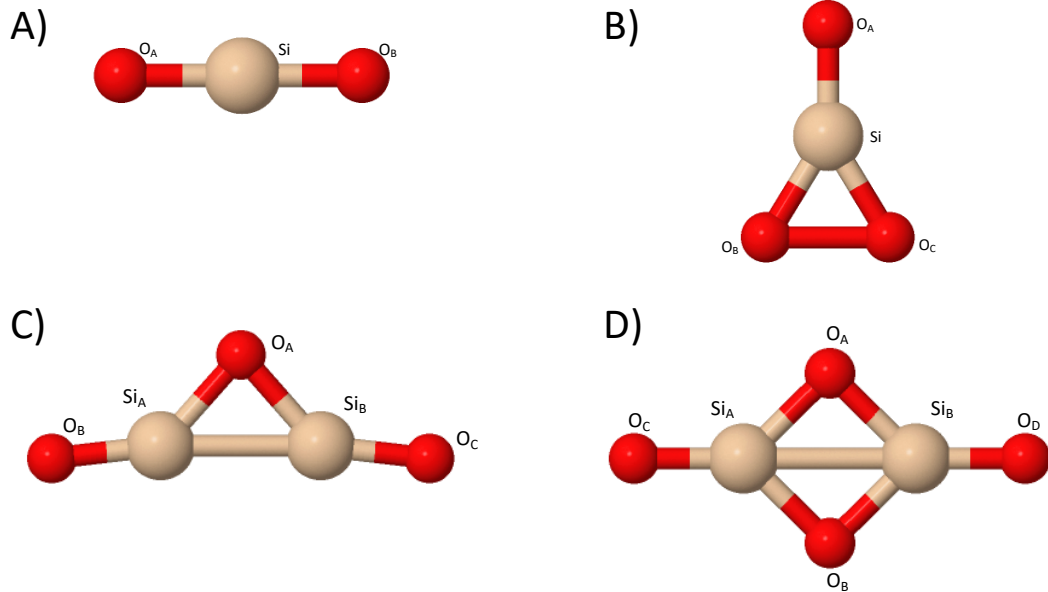
58 attributions. Most notably, the a_1 O–O stretch could not be attributed experimentally
 59 from the DFT computations. The larger structures have been observed through photo-
 60 electron spectroscopy (Wang et al., 1996, 1997), but the fundamental vibrational frequen-
 61 cies have not been conclusively determined in the laboratory. Three modes of Si_2O_4 have
 62 been reported in the literature again from argon matrix experiments (Mehner et al., 1980),
 63 but there has been no experimental or high-level theoretical follow-up in the interven-
 64 ing 30 years. Granted, the gas phase data are likely similar to the argon matrix results
 65 in each of these studies since the argon should interact far less with the silicon and oxy-
 66 gen atoms than they would with hydrogens, for instance, but corroboration of some va-
 67 riety for these modes is still lacking. While some are better understood than others, the
 68 full vibrational spectra and especially gas-phase rotational constants for each these molecules
 69 are not fully classified.

70 Consequently, high-accuracy spectroscopic predictions for the vibrational frequen-
 71 cies of these molecules will enhance spectral models of environments where they may be
 72 found both in the laboratory and in nature. Quartic force fields (QFFs) are fourth-order
 73 Taylor series approximations to the potential portion of the internuclear Hamiltonian
 74 (Fortenberry & Lee, 2019). These have been shown to produce exceptional accuracy for
 75 determining anharmonic vibrational frequencies for relatively low computational cost,
 76 provided that a sufficient electronic structure method can be used to compute this spe-
 77 cialized potential energy surface (Fortenberry & Lee, 2019), most often coupled cluster
 78 theory at the singles, doubles, and perturbative triples [CCSD(T)](Raghavachari et al.,
 79 1989; Shavitt & Bartlett, 2009) level. The most accurate QFFs have produced vibrational
 80 frequencies to within 1 cm^{-1} on occasion and most often within $5\text{--}10 \text{ cm}^{-1}$. The accu-
 81 racy of the rotational constants vary, but most are within 30 MHz of gas phase exper-
 82 iment (Huang & Lee, 2008, 2009; Huang et al., 2011; Fortenberry et al., 2011a, 2011b,
 83 2012; Huang et al., 2013; Fortenberry et al., 2014; Zhao et al., 2014; Fortenberry et al.,
 84 2015; Kitchens & Fortenberry, 2016; Fortenberry, 2017; Bizzocchi et al., 2017).

85 However, the computational cost of this involved CCSD(T) approach including cor-
 86 rections for core electron correlation and complete basis set extrapolations is prohibitive
 87 for molecules containing more than five atoms. Recent work has shown that vibrational
 88 frequencies of closed-shell molecules utilizing explicitly correlated CCSD(T)-F12b(Adler
 89 et al., 2007; Knizia et al., 2009) for the QFF energy points are within 7 cm^{-1} of the more
 90 expensive computations and cost orders of magnitude less time (Agbaglo et al., 2019;
 91 Agbaglo & Fortenberry, 2019a, 2019b). Some CCSD(T)-F12b anharmonic vibrational
 92 frequencies are actually closer to experiment than their more costly counterparts (Agbaglo
 93 & Fortenberry, 2019a). This approach has been utilized to predict anharmonic spectral
 94 data for MgSiO_3 and two isomers of Mg_2SiO_4 (enstatite and forsterite monomers, re-
 95 spectively) for which no previous vibrational or rotational spectroscopic data, theoret-
 96 ical or otherwise, exist (Valencia et al., 2020). Most notably these inorganic oxides pro-
 97 duce very large infrared intensities implying that relatively small amounts of material
 98 could still be observed (Kloska & Fortenberry, 2018; Palmer & Fortenberry, 2018; Va-
 99 lencia et al., 2020; Westbrook & Fortenberry, 2020). Furthermore, other studies have pro-
 100 duced scaling factors for harmonic frequencies of small, inorganic oxides that promise
 101 to reduce the computational time further for similar species in the production of accu-
 102 rate, anharmonic vibrational frequencies (Westbrook & Fortenberry, 2020).

103 Regardless, the present work will extend the data for these geophysically- and astrochemically-
 104 relevant silicon oxides by computing the anharmonic vibrational frequencies and spec-
 105 troscopic constants for four silicon oxide structures: SiO_2 , SiO_3 , Si_2O_3 , and Si_2O_4 . The
 106 D_{3h} structures of both CO_3 and SiO_3 have proven problematic in the past (Beste & Bartlett,
 107 2002). Here, only the C_{2v} SiO_3 structure, akin to its carbon analogue which performed
 108 well in recent QFF examination (Fortenberry et al., 2019), is considered. The D_{2h} struc-
 109 ture of Si_2O_4 has also been previously imposed to explain the results of photoelectron
 110 experiments (Wang et al., 1996) and the known vibrational frequencies thereof (Mehner

Figure 1. The optimized geometries and atom labels of A) SiO_2 , B) SiO_3 , C) Si_2O_3 , and D) Si_2O_4 .



et al., 1980). The rovibrational data provided herein will help to classify the building blocks or end products of silicates in regions where the solid form is known to exist (Rho et al., 2018; McCarthy et al., 2019) especially with the growth in telescopic power most notably signified in the upcoming launch of the *James Webb Space Telescope (JWST)*.

2 Computational Details

Precise optimization of the reference geometry is the first step to computing QFF-based anharmonic rovibrational data. The geometry optimization and all subsequent energy computations use CCSD(T)-F12b with the cc-pVTZ-F12 (Hill & Peterson, 2010; Prascher et al., 2011) basis set (abbreviated as F12-TZ from here on) in MOLPRO2015.1 (Werner et al., 2015, 2012). The optimized geometry is then used to compute the harmonic vibrational frequencies within MOLPRO for comparison to those that result from the QFF. From the reference geometry of each silicon oxide molecule, coordinates are constructed to define the QFF with the bond lengths displaced by 0.005 Å and the bond angles and dihedrals displaced by 0.005 radians. Each of the four molecules has its own unique coordinate system since each has a different number of bond lengths, angles, and dihedrals giving different numbers of total points necessary for the QFF. SiO_2 has 57; SiO_3 has 413; Si_2O_3 has 1585; and Si_2O_4 has 1973 points. The coordinates for each system are defined below with atom labels in Figure 1. The out-of-plane torsional modes are labeled as OPB. The coordinates for SiO_2 :

$$S_1(\sigma_g) = \frac{1}{\sqrt{2}}[(\text{Si} - \text{O}_A) + (\text{Si} - \text{O}_B)] \quad (1)$$

$$S_2(\sigma_u) = \frac{1}{\sqrt{2}}[(\text{Si} - \text{O}_A) - (\text{Si} - \text{O}_B)] \quad (2)$$

$$S_3(\pi_u) = \angle(\text{O}_A - \text{Si} - \text{O}_B) \quad (3)$$

$$S_4(\pi_u) = \angle(\text{O}_A - \text{Si} - \text{O}_B); \quad (4)$$

130 SiO₃

$$S_1(a_1) = Si - O_A \quad (5)$$

$$S_2(a_1) = \frac{1}{\sqrt{2}}[(O_B - Si) + (O_C - Si)] \quad (6)$$

$$S_3(a_1) = \frac{1}{\sqrt{2}}[\angle(O_B - Si - O_A) + \angle(O_C - Si - O_A)] \quad (7)$$

$$S_4(b_2) = \frac{1}{\sqrt{2}}[(O_B - Si) - (O_C - Si)] \quad (8)$$

$$S_5(b_2) = \frac{1}{\sqrt{2}}[\angle(O_B - Si - O_A) - \angle(O_C - Si - O_A)] \quad (9)$$

$$S_6(b_1) = OPB(O_A - Si - O_B - O_C); \quad (10)$$

131 Si₂O₃

$$S_1(a_1) = Si_1 - Si_2 \quad (11)$$

$$S_2(a_1) = \frac{1}{\sqrt{2}}[(O_A - Si_A) + (O_A - Si_B)] \quad (12)$$

$$S_3(a_1) = \frac{1}{\sqrt{2}}[(Si_A - O_B) + (Si_B - O_C)] \quad (13)$$

$$S_4(a_1) = \frac{1}{\sqrt{2}}[\angle(O_B - Si_A - O_A) + \angle(O_C - Si_B - O_A)] \quad (14)$$

$$S_5(b_2) = \frac{1}{\sqrt{2}}[(O_A - Si_A) - (O_A - Si_B)] \quad (15)$$

$$S_6(b_2) = \frac{1}{\sqrt{2}}[(Si_A - O_B) - (Si_B - O_C)] \quad (16)$$

$$S_7(b_2) = \frac{1}{\sqrt{2}}[\angle(O_B - Si_A - O_A) - \angle(O_C - Si_B - O_A)] \quad (17)$$

$$S_8(b_1) = \frac{1}{\sqrt{2}}[\tau(O_B - Si_A - O_A - Si_B) - \tau(O_C - Si_B - O_A - Si_A)] \quad (18)$$

$$S_9(a_2) = \frac{1}{\sqrt{2}}[\tau(O_B - Si_A - O_A - Si_B) + \tau(O_C - Si_B - O_A - Si_A)]; \quad (19)$$

132 and Si₂O₄

$$S_1(a_g) = \frac{1}{\sqrt{2}}[(O_A - O_B) + (Si_A - Si_B)] \quad (20)$$

$$S_2(a_g) = \frac{1}{\sqrt{2}}[(O_A - O_B) - (Si_A - Si_B)] \quad (21)$$

$$S_3(a_g) = \frac{1}{\sqrt{2}}[(Si_A - O_C) + (Si_B - O_D)] \quad (22)$$

$$S_4(b_{1u}) = \frac{1}{2}[(O_A - Si_A) - (O_A - Si_B) - (O_B - Si_A) + (O_B - Si_B)] \quad (23)$$

$$S_5(b_{1u}) = \frac{1}{2}[\angle(O_C - Si_A - O_A) - \angle(O_C - Si_A - O_B) - \angle(O_D - Si_2 - O_A) + \angle(O_D - Si_B - O_B)] \quad (24)$$

$$S_6(b_{2u}) = \frac{1}{2}[(O_A - Si_A) + (O_A - Si_B) - (O_B - Si_A) - (O_B - Si_B)] \quad (25)$$

$$S_7(b_{2u}) = \frac{1}{2}[\angle(O_C - Si_A - O_A) + \angle(O_C - Si_A - O_B) - \angle(O_D - Si_2 - O_A) - \angle(O_D - Si_B - O_B)] \quad (26)$$

$$S_8(b_{3g}) = \frac{1}{\sqrt{2}}[(Si_A - O_C) - (Si_B - O_D)] \quad (27)$$

$$S_9(b_{3g}) = \frac{1}{2}[(O_A - Si_A) - (O_A - Si_B) + (O_B - Si_A) - (O_B - Si_B)] \quad (28)$$

$$S_{10}(b_{3u}) = \frac{1}{\sqrt{2}}[(O_C)_z + (O_D)_z] \quad (29)$$

$$S_{11}(b_{3u}) = \frac{1}{2}[(O_A)_z + (O_B)_z - (Si_A)_z - (Si_B)_z] \quad (30)$$

$$S_{12}(b_{2u}) = \frac{1}{\sqrt{2}}[(O_C)_z - (O_D)_z], \quad (31)$$

133 where the last of these three has exhibited some questionable results in the low-frequency
 134 range for the magnesium fluoride dimer (Palmer & Fortenberry, 2018). The other coor-
 135 dinate systems have been utilized successfully in previous studies on the magnesium hy-
 136 diide monomer, HeHHe⁺, carbon dioxide, CO₃, NCNCN⁻, and C₂O₃ (Palmer & Forten-
 137 berry, 2018; Stephan & Fortenberry, 2017; Fortenberry et al., 2019; Dubois et al., 2019).

138 The resulting energies are fit to a least-squares polynomial giving a sum of squared
 139 residuals on the order of 10⁻¹⁷ a.u.² for all molecules but Si₂O₄ which is 10⁻¹³ a.u.² This
 140 fit determines the actual minimum, or equilibrium, geometry. The final set of force con-
 141 stants are generated by refitting the points to this new minimum; these are given in the
 142 supplemental information (SI). The INTDER program (Allen & coworkers, 2005) trans-
 143 forms these force constants into Cartesian coordinates for more general implementation.
 144 Then, the SPECTRO program (Gaw et al., 1991) computes the harmonic and anhar-
 145 monic frequencies including anharmonic zero-point vibrational energies (ZPVEs) using

Table 1. The F12-TZ Geometrical Parameters (in Å or Degrees) as Defined from Figure 1.

	SiO ₂	SiO ₃	Si ₂ O ₃	Si ₂ O ₄
r_0 (Si _A –O _A)	1.51249	1.50567	1.50675	1.50045
r_0 (Si _A –O _B)		1.62024	1.67351	1.66525 ^a
\angle_0 (O _A –Si _A –O _B)		148.675	137.445	90.544
r_0 (Si _A –Si _B)			2.21681	2.36644
\angle_0 (O _A –Si _A –O _C)				135.326
r_e (Si _A –O _A)	1.51066	1.50395	1.50726	1.50337
r_e (Si _A –O _B)		1.61659	1.66903	1.66135 ^a
\angle_e (O _A –Si _A –O _B)		148.814	137.313	90.673
r_e (Si _A –Si _B)			2.21069	2.36327
\angle_e (O _A –Si _A –O _C)				135.337

^aThis is actually the r_0 (Si_A–O_C), but is placed here for consistency of bond type.

vibrational perturbation theory at second-order (VPT2) as well as spectroscopic constants making use of rotational perturbation theory at second-order (Mills, 1972; Watson, 1977; Papousek & Aliev, 1982) and Fermi resonance polyads (Martin & Taylor, 1997).

The B3LYP/aug-cc-pVDZ double-harmonic intensities and dipole moments are computed with Gaussian09 (Becke, 1993; Yang et al., 1986; Lee et al., 1988; Dunning, 1989; Frisch et al., 2009). These have been shown to be in good agreement with higher-level computations previously (Yu et al., 2015; Finney et al., 2016). Additionally, the scaling factors for the Si–O stretching (0.98242) and bending (0.99261) frequencies determined previously (Westbrook & Fortenberry, 2020) are applied to the harmonics computed directly in MOLPRO for comparison of their performance in these related but not identical systems.

3 Results & Discussion

The geometries for each of the four molecules examined here are given in Table 1 with labels from Figure 1. Most notably, the Si_A–O_A bond lengths, those that have the oxygen atom in a silaketone moiety (external Si=O group) are largely consistent with a bond length on the order of 1.5 Å. SiO₂ is the exception to this where the longer bond length likely arises from the weakening of the silicon atom's electron donation due to having two Si=O bonds instead of just one, and its magnitude here is in line with that computed previously (Tremblay et al., 1996). The Si_A–O_{B/C} bonds can be thought of as single bonds from a carbon analogue (Fortenberry et al., 2019) and are notably and consistently longer. The Si–Si bonds are longer in Si₂O₄ than in Si₂O₃, but the additional oxygen atom in the former naturally increases the size of the ring thus making for a longer diagonal distance between silicon atoms.

3.1 Anharmonic Frequencies

The F12-TZ vibrational frequencies for SiO₂ are given in Table 2. While the gas phase values for this molecule are not known, the argon matrix results correlate exceptionally well with the explicit QFF values for the 1420.7 cm⁻¹ and 289.0 cm⁻¹ fundamentals compared to the 1416 cm⁻¹ and 273 cm⁻¹ experimental frequencies (Jacox, 1994). Interestingly, the scaled 1414.4 cm⁻¹ and 288.5 cm⁻¹ frequencies for the same modes are in slightly closer agreement with experiment. Even so, the difference in the explicit QFF anharmonic frequencies and the scaled values are within the accuracy (7 cm⁻¹) of the F12-TZ approach implying that either is a valuable choice of method. The vibrationally-

Table 2. The F12-TZ Vibrational Frequencies (in cm^{-1}) and Intensities (in km/mol) for SiO_2 .

Mode	Description	Symmetry	Frequency	Exp. ^a	Scaled	$\Delta(\text{QFF-Scaled})$
ω_1	Si–O antisymm. stretch	(σ_u)	1439.7 (67)			
ω_2	Si–O symm. stretch	(σ_g)	992.4 (0)			
ω_3	O–Si–O bend	(π_u)	290.6 (79)			
ZPVE	1501.9					
ν_1	Si–O antisymm. stretch	(σ_u)	1420.7	1416	1414.4	6.3
ν_2	Si–O symm. stretch	(σ_g)	984.2		975.0	9.2
ν_3	O–Si–O bend	(π_u)	289.0	273	288.5	0.5

^aArgon matrix experimental data from (H. Schnöckel, 1978; V. H. Schnöckel, 1980;
Andrews & McCluskey, 1992; Jacox, 1994)

Table 3. The F12-TZ QFF Vibrational Frequencies (cm^{-1}) and Intensities (km/mol) for C_{2v} SiO_3 .

Mode	Description	Symmetry	Frequency	Exp. ^a	Scaled	$\Delta(\text{QFF-Scaled})$
ω_1	Si-O _A	a ₁	1391.4 (114)			
ω_2	Si-O _B + Si-O _C	a ₁	894.2 (5)			
ω_3	Si-O _B - Si-O _C	b ₂	868.5 (90)			
ω_4	$\angle \text{O}_A\text{-Si-O}_B + \angle \text{O}_A\text{-Si-O}_C$	a ₁	515.0 (25)			
ω_5	Si OPB	b ₁	309.7 (82)			
ω_6	$\angle \text{O}_A\text{-Si-O}_B - \angle \text{O}_A\text{-Si-O}_C$	b ₂	299.3 (60)			
ZPVE	2129.5					
ν_1	Si-O _A	a ₁	1371.0	1363.5 (100)	1366.9	4.1
ν_2	Si-O _B + Si-O _C	a ₁	885.3	877.1 (12)	878.5	6.8
ν_3	Si-O _B - Si-O _C	b ₂	857.1	855.3 (53)	853.2	3.9
ν_4	$\angle \text{O}_A\text{-Si-O}_B + \angle \text{O}_A\text{-Si-O}_C$	a ₁	497.0	–	511.2	-14.2
ν_5	Si OPB	b ₁	305.3	287.8 (96)	307.4	-2.1
ν_6	$\angle \text{O}_A\text{-Si-O}_B - \angle \text{O}_A\text{-Si-O}_C$	b ₂	298.0	292.0 (62)	297.1	0.9

^aArgon matrix data from (Tremblay et al., 1996).

dark symmetric stretch has a larger difference between the two anharmonic frequencies, but no experimental data can verify which is more accurate. The F12-TZ QFF produces nearly identical values as gas-phase experimental CO_2 frequencies (differences of less than 2 cm^{-1} in every case) (Fortenberry et al., 2019), and similar accuracies appear to be present in the silicon analogue, as well.

The strong correspondence between theory and argon matrix experiments continues with C_{2v} SiO_3 . As shown in Table 3, the difference between the F12-TZ SiO_3 anharmonic frequencies and that for the argon matrix experiments (Tremblay et al., 1996) is never more than 8 cm^{-1} , and ν_3 at 857.1 cm^{-1} is within 2 cm^{-1} of experiment. Granted, the matrix will shift these values relative to the gas phase values that would be observed in astrophysical contexts, but, again, these shifts should be small. Furthermore, the B3LYP/aug-cc-pVTZ double-harmonic intensities are in at least semi-quantitative agreement with experiment showing which bands could be considered strong and which could be considered weak. Unsurprisingly, the ν_1 terminal Si=O_A stretch at 1371.0 cm^{-1} is the brightest vibrational mode, and the OPB bend for O_A is also bright lining up with experiment.

Table 4. Si_2O_3 F12-TZ Harmonic and Fundamental Vibrational Frequencies (in cm^{-1}) and B3LYP Intensities (in km/mol).

Mode	Description	Symmetry	Frequency	Scaled	$\Delta(\text{QFF-Scaled})$
ω_1	$\text{Si}_A\text{-O}_B + \text{Si}_B\text{-O}_C$	a ₁	1331.0 (17)		
ω_2	$\text{Si}_A\text{-O}_B - \text{Si}_B\text{-O}_C$	b ₂	1274.0(152)		
ω_3	$\text{Si}_A\text{-O}_A + \text{Si}_B\text{-O}_A$	a ₁	859.1(122)		
ω_4	$\text{Si}_A\text{-O}_A - \text{Si}_B\text{-O}_A$	b ₂	663.2(52)		
ω_5	$\text{Si}_A\text{-Si}_B$	a ₁	440.7(21)		
ω_6	$\angle \text{O}_A\text{-Si}_A\text{-O}_B - \angle \text{O}_A\text{-Si}_B\text{-O}_C$	b ₂	248.7(16)		
ω_7	$\tau(\text{O}_B\text{-Si}_A\text{-O}_A\text{-Si}_B) + \tau(\text{O}_C\text{-Si}_B\text{-O}_A\text{-Si}_A)$	b ₁	245.7(62)		
ω_8	$\angle \text{O}_A\text{-Si}_A\text{-O}_B + \angle \text{O}_A\text{-Si}_B\text{-O}_C$	a ₁	189.8(30)		
ω_9	$\tau(\text{O}_B\text{-Si}_A\text{-O}_A\text{-Si}_B) + \tau(\text{O}_C\text{-Si}_B\text{-O}_A\text{-Si}_A)$	a ₂	153.4(0)		
ZPVE			2679.5		
ν_1	$\text{Si}_A\text{-O}_B + \text{Si}_B\text{-O}_C$	a ₁	1303.3	1307.6	-4.3
ν_2	$\text{Si}_A\text{-O}_B - \text{Si}_B\text{-O}_C$	b ₂	1245.6	1251.6	-6.0
ν_3	$\text{Si}_A\text{-O}_A + \text{Si}_B\text{-O}_A$	a ₁	836.2	844.0	-7.8
ν_4	$\text{Si}_A\text{-O}_A - \text{Si}_B\text{-O}_A$	b ₂	637.6	651.6	-14.0
ν_5	$\text{Si}_A\text{-Si}_B$	a ₁	432.5	437.5	-5.0
ν_6	$\angle \text{O}_A\text{-Si}_A\text{-O}_B - \angle \text{O}_A\text{-Si}_B\text{-O}_C$	b ₂	245.0	246.9	-1.9
ν_7	$\tau(\text{O}_B\text{-Si}_A\text{-O}_A\text{-Si}_B) + \tau(\text{O}_C\text{-Si}_B\text{-O}_A\text{-Si}_A)$	b ₁	244.6	243.9	0.7
ν_8	$\angle \text{O}_A\text{-Si}_A\text{-O}_B + \angle \text{O}_A\text{-Si}_B\text{-O}_C$	a ₁	188.2	188.4	-0.2
ν_9	$\tau(\text{O}_B\text{-Si}_A\text{-O}_A\text{-Si}_B) + \tau(\text{O}_C\text{-Si}_B\text{-O}_A\text{-Si}_A)$	a ₂	153.7	152.3	1.4

The previous SiO_3 experiment could not identify the $a_1 \nu_4$ symmetric bend (equivalently described as the O–O stretch). This fundamental has an intensity greater than the ν_2 Si–O symmetric stretch previously characterized in the argon matrix experiments (Tremblay et al., 1996). The reason is likely that the previous DFT computations suggested that the fundamental should lie higher in frequency close to 582 cm^{-1} . However, the present work strongly suggests that this fundamental is much lower in frequency at 497.0 cm^{-1} . Unfortunately, this region of the IR spectrum is not reported in this previous work negating any *ex post facto* analysis. Regardless, the F12-TZ QFF values confirm the other argon matrix fundamental vibrational frequency assignments for C_{2v} SiO_3 (Tremblay et al., 1996) and show that the last remaining band is most likely lower in frequency than previously believed.

The F12-TZ QFF fundamental vibrational frequencies for Si_2O_3 have not been previously explored experimentally or theoretically and are given here in Table 4. The silaketon stretches (ν_1 and ν_2) are in the same frequency range as that for SiO_3 , and the antisymmetric ν_2 stretch at 1245.6 cm^{-1} has the greatest intensity of all the fundamentals. This is also true for the related C_2O_3 and C_2N_3^- molecules (Fortenberry et al., 2019; Dubois et al., 2019). The $a_1 \nu_3$ stretching of the central O_A atom produces the next-brightest fundamental at 836.2 cm^{-1} . The permanent dipole moment is being extended in this case, giving a larger charge separation upon vibration. The remaining frequencies are dimer but still non-negligible, and the five lowest frequency fundamentals are all below 500 cm^{-1} , as is common for such heavy atoms like silicon (Kloska & Fortenberry, 2018; Palmer & Fortenberry, 2018; Valencia et al., 2020).

The 12 fundamental vibrational frequencies for D_{2h} Si_2O_4 are given in Table 5. The silaketon stretches are blue-shifted in this molecule compared to Si_2O_3 and are present above 1300 cm^{-1} . The b_{3g} ν_2 antisymmetric stretch, again, has the largest intensity of

Table 5. Si_2O_4 F12-TZ Harmonic and Fundamental Vibrational Frequencies (in cm^{-1}) and B3LYP Intensities (in km/mol).

Mode	Description	Symmetry	Frequency	Exp. ^a	Scaled	$\Delta(\text{QFF-Scaled})$
ω_1	$\text{Si}_A-\text{O}_C + \text{Si}_B-\text{O}_D$	a_g	1354.4 (0)			
ω_2	$\text{Si}_A-\text{O}_C - \text{Si}_B-\text{O}_D$	b_{3g}	1316.9 (382)			
ω_3	$\text{Si}_A-\text{O}_B + \text{Si}_B-\text{O}_B - \text{Si}_A-\text{O}_A - \text{Si}_B-\text{O}_A$	b_{2u}	904.8 (259)			
ω_4	$\text{O}_A-\text{O}_B + \text{Si}_A-\text{Si}_B$	a_g	871.6 (0)			
ω_5	$\text{O}_B-\text{Si}_A - \text{O}_B-\text{Si}_B + \text{O}_A-\text{Si}_A - \text{O}_A-\text{Si}_B$	b_{3g}	804.0 (252)			
ω_6	$\text{O}_B-\text{Si}_A - \text{O}_B-\text{Si}_B - \text{O}_A-\text{Si}_A + \text{O}_A-\text{Si}_B$	b_{1u}	718.7 (0)			
ω_7	$\text{O}_A-\text{O}_B - \text{Si}_A-\text{Si}_B$	a_g	488.0 (0)			
ω_8	Symm. O_A-O_B OPB	b_{3u}	465.4 (99)			
ω_9	$\text{O}_C-\text{Si}_A-\text{O}_B - \text{O}_C-\text{Si}_A-\text{O}_A + \text{O}_D-\text{Si}_B-\text{O}_B + \text{O}_D-\text{Si}_B-\text{O}_A$	b_{1u}	313.3 (0)			
ω_{10}	$\text{O}_C-\text{Si}_A-\text{O}_B - \text{O}_C-\text{Si}_A-\text{O}_A + \text{O}_D-\text{Si}_B-\text{O}_B - \text{O}_D-\text{Si}_B-\text{O}_A$	b_{2u}	295.5 [†] (43)			
ω_{11}	Antisymm. O_C/O_D OPB	b_{2u}	236.6 (0)			
ω_{12}	Symm. O_C/O_D OPB	b_{3u}	121.5 [†] (26)			
ZPVE			3796.3			
ν_1	$\text{Si}_A-\text{O}_C + \text{Si}_B-\text{O}_D$	a_g	1338.2		1330.6	7.6
ν_2	$\text{Si}_A-\text{O}_C - \text{Si}_B-\text{O}_D$	b_{3g}	1303.6	1293.3	1293.7	9.9
ν_3	$\text{Si}_A-\text{O}_B + \text{Si}_B-\text{O}_B - \text{Si}_A-\text{O}_A - \text{Si}_B-\text{O}_A$	b_{2u}	911.7	889.2	888.9	22.8
ν_4	$\text{O}_A-\text{O}_B + \text{Si}_A-\text{Si}_B$	a_g	861.3		856.3	5.0
ν_5	$\text{O}_B-\text{Si}_A - \text{O}_B-\text{Si}_B + \text{O}_A-\text{Si}_A - \text{O}_A-\text{Si}_B$	b_{3g}	856.8	786.4	789.9	66.9
ν_6	$\text{O}_B-\text{Si}_A - \text{O}_B-\text{Si}_B - \text{O}_A-\text{Si}_A + \text{O}_A-\text{Si}_B$	b_{1u}	658.1		706.1	-48.0
ν_7	$\text{O}_A-\text{O}_B - \text{Si}_A-\text{Si}_B$	a_g	485.9		479.4	6.5
ν_8	Symm. O_A-O_B OPB	b_{3u}	456.1		462.0	-5.9
ν_9	$\text{O}_C-\text{Si}_A-\text{O}_B - \text{O}_C-\text{Si}_A-\text{O}_A + \text{O}_D-\text{Si}_B-\text{O}_B + \text{O}_D-\text{Si}_B-\text{O}_A$	b_{1u}	281.7		311.0	-29.3
ν_{10}	$\text{O}_C-\text{Si}_A-\text{O}_B - \text{O}_C-\text{Si}_A-\text{O}_A + \text{O}_D-\text{Si}_B-\text{O}_B - \text{O}_D-\text{Si}_B-\text{O}_A$	b_{2u}			293.3	
ν_{11}	Antisymm. O_C/O_D OPB	b_{2u}	230.5		234.9	-4.4
ν_{12}	Symm. O_C/O_D OPB	b_{3u}			120.6	

^a Argon matrix experimental results from (Mehner et al., 1980). [†] Denotes a MOLPRO harmonic frequency

all the fundamental frequencies for this molecule. Stretches within the ring (ν_3 and ν_5) are the next-brightest with intensities above 250 km/mol, more than 3.5 times that of the antisymmetric stretch in water. Comparison to argon matrix data from (Mehner et al., 1980) gives good agreement between the 1293.3 cm^{-1} value and the F12-TZ QFF ν_2 frequency at 1303.6 cm^{-1} . This deteriorates slightly for ν_3 where experiment places this at 889.2 cm^{-1} and the QFF is 911.7 cm^{-1} . The correlation is completely off for ν_5 with experiment attributing this ring deformation to a band at 786.4 cm^{-1} and the QFF at 856.8 cm^{-1} . Either the band has been misassigned in the experiment, or the computations are off.

In this case, the latter is most likely correct. The fitting of the points was the worst for Si_2O_4 of the silicon oxides studied. Furthermore, two harmonic vibrational frequencies computed via the QFF do not align with those computed from within MOLPRO's standard harmonic frequency computation, ω_{10} and ω_{12} . The OPB coordinate struggles to define the proper motion within the constraints of the QFF and VPT2, and this subsequently affects the fitting of the force constants for the other coordinates. The potential for the OPB is likely flat reducing the capabilities of VPT2 as defined by the QFF. The ν_{10} and ν_{12} fundamentals could not even be computed from the QFF data. Hence, the F12-TZ QFF VPT2 anharmonic vibrational frequencies for Si_2O_4 below the silaketon stretches should be treated as suggestions.

However, all is not lost in the prediction of these anharmonic frequencies. The recent determination of scaling factors for M–O stretches and bends (where M is a second-row atom) can be applied to Si_2O_4 . Doing so actually produces a fundamental frequency for ν_3 at 888.9 cm^{-1} and ν_5 at 789.9 cm^{-1} . Both are within 3.5 cm^{-1} of the argon matrix experiment. Furthermore, the ν_2 antisymmetric stretch is 1293.7 cm^{-1} from the scaled values, 9.9 cm^{-1} below the explicit QFF, and only 0.4 cm^{-1} below the experimental value. Consequently, the scaled harmonics are likely producing more meaningful fundamental vibrational frequencies for this molecule than the QFF. The harmonic force field is much better behaved and less likely to suffer from noise contamination in these numerical derivatives (Huang & Lee, 2008, 2009), and the amount of absolute anharmonicity is relatively small in the first place.

The scaled harmonic frequencies are also listed for the other three molecules giving slightly better correlation with experiment for SiO_2 (Table 2) as discussed previously. Agreement between experiment and scaled harmonics of SiO_3 (Table 3) is comparable with the F12-TZ QFF VPT2 results. Some modes are better with the scaled values (ν_1) and some with the explicit anharmonicity computed (ν_3) implying that either is appropriate. Both also demonstrate that ν_4 is still lower in frequency than previous experiments explored. Since there are no experimental data for Si_2O_3 , comparison between the QFF VPT2 results and the scaled harmonics both with F12-TZ is necessary, but both are quite comparable with one another (Table 4). All modes agree to within 8 cm^{-1} save for the b_2 ν_4 antisymmetric stretch. The mean absolute error (MAE) between the QFF and scaled harmonics for the stretching frequencies is 5.8 cm^{-1} when removing ν_4 and 8.0 cm^{-1} when including it. The bends and torsions are much closer with the MAE at 1.8 cm^{-1} , but, again, the magnitudes of the frequencies are smaller in the first place. Hence, these scaling factors are comparable to the QFF VPT2 fundamental vibrational frequencies implying that these heuristics could be used as a first-order guess to the fundamental vibrational frequencies of Si_2O_4 and potentially even for larger silicon oxide clusters where QFFs or any anharmonic vibrational frequency computations are prohibitively large.

3.2 Rotational and Spectroscopic Constants

The spectroscopic constants for each of the molecules examined are given in Table 6. These include the pure rotational constants, the vibrationally-averaged rotational constants, the quartic and sextic (Watson S Hamiltonian) distortion constants, and even

Table 6. The F12-TZ QFF Spectroscopic Data for the Four Silicon Oxides.

	SiO ₂	SiO ₃	Si ₂ O ₃	Si ₂ O ₄
<i>A</i> ₀ (MHz)		22360.3	21364.6	11474.0
<i>B</i> ₀ (MHz)	6907.7	5489.9	1766.6	1636.1
<i>C</i> ₀ (MHz)		4400.5	1630.8	1433.1
<i>A</i> ₁ (MHz)		22333.1	21390.3	11469.1
<i>B</i> ₁ (MHz)	6872.3	5466.1	1761.6	1632.6
<i>C</i> ₁ (MHz)		4384.4	1626.6	1430.4
<i>A</i> ₂ (MHz)		22292.4	21361.1	11465.8
<i>B</i> ₂ (MHz)	6888.1	5480.1	1762.9	1633.0
<i>C</i> ₂ (MHz)		4392.0	1627.6	1430.8
<i>A</i> ₃ (MHz)		22446.5	21282.1	11497.3
<i>B</i> ₃ (MHz)	6920.3	5469.6	1764.8	1633.3
<i>C</i> ₃ (MHz)		4391.4	1628.1	1430.4
<i>A</i> ₄ (MHz)		22001.5	20997.0	11458.5
<i>B</i> ₄ (MHz)		5518.5	1768.1	1635.0
<i>C</i> ₄ (MHz)		4392.3	1629.6	1431.8
<i>A</i> ₅ (MHz)		22310.3	21576.9	11442.8
<i>B</i> ₅ (MHz)		5493.9	1761.6	1635.2
<i>C</i> ₅ (MHz)		4409.0	1627.2	1431.5
<i>A</i> ₆ (MHz)		22408.0	21370.4	11446.5
<i>B</i> ₆ (MHz)		5504.1	1768.2	1633.6
<i>C</i> ₆ (MHz)		4400.9	1631.2	1430.7
<i>A</i> ₇ (MHz)			21368.9	
<i>B</i> ₇ (MHz)			1767.8	
<i>C</i> ₇ (MHz)			1632.6	
<i>A</i> ₈ (MHz)			21507.1	
<i>B</i> ₈ (MHz)			1767.9	
<i>C</i> ₈ (MHz)			1630.7	
<i>A</i> ₉ (MHz)			21279.8	
<i>B</i> ₉ (MHz)			1768.2	
<i>C</i> ₉ (MHz)			1633.4	
Δ_J (Hz)	1.500	941.78	120.62	56.658
Δ_K (kHz)		133.62	363.47	9.985
Δ_{JK} (kHz)		15.616	-4.444	0.389
δ_J (Hz)		227.57	18.119	8.426
δ_K (kHz)		11.708	1.065	0.484
Φ_J (μ Hz)	-8.885	518.99	2.540	2.770
Φ_K (Hz)		-0.240	9.387	0.022
Φ_{JK} (mHz)		80.382	0.920	0.242
Φ_{KJ} (mHz)		-233.60	-127.77	-4.098
ϕ_j (μ Hz)		261.21	4.481	1.058
ϕ_{jk} (mHz)		45.749	0.152	0.152
ϕ_k (Hz)		1.292	0.502	0.009
μ (D)		—	0.87	0.66
			—	—

the dipole moments of the two C_{2v} molecules. While these may not be as accurate as methods including core electron correlation or other additive factors (Agbaglo & Fortenberry, 2019a, 2019b), these rotational constants should serve as a good starting point for assessing the rotational spectra of these molecules. Strangely, a search of the literature did not yield any experimental rotational constants for SiO_2 which are provided here for this nonpolar molecule. The other three molecules are all clearly near-prolate rotors especially for Si_2O_3 .

The vibrationally-excited rotational constants (numbered in the same order as the fundamental vibrational frequencies) for Si_2O_4 are given for the modes with the least questionable vibrational frequencies. While the pure rotational transitions of this molecule will not be observed since it has no dipole moment, the A_2 , B_2 , and C_2 values, however, will likely be important for rovibrational modeling since ν_2 of this molecule has the largest infrared intensity computed of the set. Finally, the dipole moments are reported at the bottom of Table 6. SiO_3 is the most polar, but Si_2O_3 has a smaller but similar magnitude dipole moment. This differs from the carbon analogues where C_2O_3 is almost apolar (Fortenberry et al., 2019) likely due to the larger electronegativity difference between oxygen and silicon as well as the longer Si–O bonds.

4 Conclusions

The small silicon oxide clusters SiO_2 , SiO_3 , Si_2O_3 , and Si_2O_4 are shown here to be stable species with notably bright mid- to far-IR active fundamental vibrational frequencies. The antisymmetric silaketone stretch in the silicon dioxide dimer has the largest intensity of the set. The range between 1420 cm^{-1} and 1250 cm^{-1} ($7.0 \mu\text{m}$ and $8.0 \mu\text{m}$) contains this most intense band and its counterparts from the other three oxides. The other infrared bands typically fall below 700 cm^{-1} ($>14.3 \mu\text{m}$) with many of the silicon oxides analyzed here having one or two bands around 850 cm^{-1} ($\sim 11.8 \mu\text{m}$). Each of these regions have notable bumps from astronomical spectra (Molster et al., 2001), implying that small, geochemically-relevant silicon oxides may be present in circumstellar media and protoplanetary disks. Upcoming *JWST* spectra could potentially resolve such peaks. The polar SiO_3 and Si_2O_3 clusters could be observed from the ground with radiotelescopes, and the present data will aid in the experimental characterization necessary to provide reference data for such observations.

Additionally, the previously derived scaling factors (Westbrook & Fortenberry, 2020) show promise in treating similar inorganic oxides that are intractable for QFF computations. Comparison to experimental spectra for SiO_2 and SiO_3 shows that both the explicit anharmonic computations and the scaled harmonics are similarly accurate partly due to the small magnitudes of the anharmonicities of the molecules examined. However, these scaled harmonics also do not suffer from coordinate issues observed in Si_2O_4 making them also potentially useful for future exploration of larger mineralogically-relevant inorganic oxides.

Acknowledgements

The authors acknowledge funding from the NSF (OIA-1757220), NASA (NNX17AH15G), and the University of Mississippi start-up funds. Datasets for this research are included in this paper (and its supplementary information files).

References

- Adler, T. B., Knizia, G., & Werner, H.-J. (2007). A simple and efficient CCSD(T)-F12 approximation. *J. Chem. Phys.*, *127*, 221106.
- Agbaglo, D., & Fortenberry, R. C. (2019a). The performance of CCSD(T)-F12/aug-

- 316 cc-pVTZ for the computation of anharmonic fundamental vibrational frequencies. *Int. J. Quantum Chem.*, *119*, e25899.
- 317
- 318 Agbaglo, D., & Fortenberry, R. C. (2019b). The performance of explicitly correlated
319 wavefunctions [CCSD(T)-F12b] in the computation of anharmonic vibrational
320 frequencies. *Chem. Phys. Lett.*, *734*, 136720.
- 321 Agbaglo, D., Lee, T. J., Thackston, R., & Fortenberry, R. C. (2019). A small
322 molecule with pah vibrational properties and a detectable rotational spectrum:
323 *c*-(C)C₃H₂, cyclopropenylidene carbene. *Astrophys. J.*, *871*, 236.
- 324 Allen, W. D., & coworkers. (2005). (*INTDER* 2005 is a General Program Written by W. D. Allen and Coworkers, which Performs Vibrational Analysis and
325 Higher-Order Non-Linear Transformations.)
- 326 Andrews, L., & McCluskey, M. (1992). Bending modes of SiO₂ and GeO₂ in solid
327 argon. *J. Mol. Spectrosc.*, *154*, 223-225.
- 328 Becke, A. D. (1993). Density-functional thermochemistry. iii. the role of exact ex-
329 change. *J. Chem. Phys.*, *98*, 5648-5652.
- 330 Beste, A., & Bartlett, R. J. (2002). The electronic structure of SiO₃: A problematic
331 example for coupled cluster methods. *Chem. Phys. Lett.*, *366*, 100-108.
- 332 Bizzocchi, L., Lattanzi, V., Laas, J., Spezzano, S., Giuliano, B. M., Prudenzano, D.,
333 ... Caselli, P. (2017). Accurate sub-millimetre rest frequencies for HOCO⁺
334 and DOCO⁺ ions. *Astron. Astrophys.*, *602*, A34.
- 335 Dubois, D., Sciamma-O'Brien, E., & Fortenberry, R. C. (2019). The fundamental
336 vibrational frequencies and spectroscopic constants of the dicyanoamine anion,
337 ncncn⁻ (c₂n₃⁻): Quantum chemical analysis for astrophysical and planetary
338 environments. *Astrophys. J.*, *883*, 109.
- 339 Dunning, T. H. (1989). Gaussian basis sets for use in correlated molecular calcu-
340 lations. i. the atoms boron through neon and hydrogen. *J. Chem. Phys.*, *90*,
341 1007-1023.
- 342 Finney, B., Fortenberry, R. C., Francisco, J. S., & Peterson, K. A. (2016). A spec-
343 troscopic case for SPSi detection: The third-row in a single molecule. *J. Chem.*
344 *Phys.*, *145*, 124311.
- 345 Fortenberry, R. C. (2017). Quantum astrochemical spectroscopy. *Int. J. Quant.*
346 *Chem.*, *117*, 81-91.
- 347 Fortenberry, R. C. (2020). The case for gas-phase astrochemistry without carbon.
348 *Mol. Astrophys.*, *18*, 100062.
- 349 Fortenberry, R. C., Huang, X., Crawford, T. D., & Lee, T. J. (2014). Quartic force
350 field rovibrational analysis of protonated acetylene, C₂H₃⁺, and its isotopo-
351 logues. *J. Phys. Chem. A*, *118*, 7034-7043.
- 352 Fortenberry, R. C., Huang, X., Francisco, J. S., Crawford, T. D., & Lee, T. J.
353 (2011a). The *trans*-HOCO radical: Fundamental vibrational frequencies,
354 quartic force fields, and spectroscopic constants. *J. Chem. Phys.*, *135*, 134301.
- 355 Fortenberry, R. C., Huang, X., Francisco, J. S., Crawford, T. D., & Lee, T. J.
356 (2011b). Vibrational frequencies and spectroscopic constants from quartic
357 force fields for *cis*-HOCO: The radical and the anion. *J. Chem. Phys.*, *135*,
358 214303.
- 359 Fortenberry, R. C., Huang, X., Francisco, J. S., Crawford, T. D., & Lee, T. J.
360 (2012). Fundamental vibrational frequencies and spectroscopic constants of
361 HOCS⁺, HSCO⁺, and isotopologues via quartic force fields. *J. Phys. Chem.*
362 *A.*, *116*, 9582-9590.
- 363 Fortenberry, R. C., & Lee, T. J. (2019). Computational vibrational spectroscopy for
364 the detection of molecules in space. *Ann. Rep. Comput. Chem.*, *15*, 173-202.
- 365 Fortenberry, R. C., Lee, T. J., & Müller, H. S. P. (2015). Excited vibrational level
366 rotational constants for SiC₂: A sensitive molecular diagnostic for astrophysi-
367 cal conditions. *Molec. Astrophys.*, *1*, 13-19.
- 368 Fortenberry, R. C., Peters, D., Ferari, B. C., & Bennett, C. J. (2019). Rovibrational
369 spectral analysis of CO₃ and C₂O₃: Potential sources for O₂ observed in comet
- 370

- 371 67P/Churyumov-Gerasimenko. *Astrophys. J. Lett.*, **886**, L10.
- 372 Frisch, M. J., Trucks, G. W., Schlegel, H. B., Scuseria, G. E., Robb, M. A., Cheeseman, J. R., ... Fox, D. J. (2009). *Gaussian 09 Revision D.01*. (Gaussian Inc. Wallingford CT)
- 373 Gaw, J. F., Willets, A., Green, W. H., & Handy, N. C. (1991). SPECTRO: A program for the derivation of spectroscopic constants from provided quartic force fields and cubic dipole fields. In J. M. Bowman & M. A. Ratner (Eds.), *Advances in molecular vibrations and collision dynamics* (p. 170-185). Greenwich, Connecticut: JAI Press, Inc.
- 374 Hill, J. G., & Peterson, K. A. (2010). Correlation consistent basis sets for explicitly correlated wavefunctions: Valence and core-valence basis sets for Li, Be, Na, and Mg. *Phys. Chem. Chem. Phys.*, **12**, 10460-10468.
- 375 Huang, X., Fortenberry, R. C., & Lee, T. J. (2013). Protonated nitrous oxide, NNOH⁺: Fundamental vibrational frequencies and spectroscopic constants from quartic force fields. *J. Chem. Phys.*, **139**(8), 084313.
- 376 Huang, X., & Lee, T. J. (2008). A procedure for computing accurate *ab initio* quartic force fields: Application to HO₂⁺ and H₂O. *J. Chem. Phys.*, **129**, 044312.
- 377 Huang, X., & Lee, T. J. (2009). Accurate *ab initio* quartic force fields for NH₂⁻ and CCH⁻ and rovibrational spectroscopic constants for their isotopologs. *J. Chem. Phys.*, **131**, 104301.
- 378 Huang, X., Taylor, P. R., & Lee, T. J. (2011). Highly accurate quartic force field, vibrational frequencies, and spectroscopic constants for cyclic and linear C₃H₃⁺. *J. Phys. Chem. A*, **115**, 5005-5016.
- 379 Jacox, M. E. (1994). Vibrational and electronic energy levels of polyatomic transient molecules. *J. Phys. Chem. Ref. Data*, **23**, 1-461.
- 380 Kitchens, M. J. R., & Fortenberry, R. C. (2016). The rovibrational nature of closed-shell third-row triatomics: HOX and HXO, X = Si⁺, P, S⁺, and Cl. *Chem. Phys.*, **472**, 119-127.
- 381 Kloska, K. A., & Fortenberry, R. C. (2018). Gas-phase spectra of MgO molecules: A possible connection from gas-phase molecules to planet formation. *Mon. Not. Royal Astron. Soc.*, **474**, 2055-2063.
- 382 Knizia, G., Adler, T. B., & Werner, H.-J. (2009). Simplified CCSD(T)-F12 Methods: Theory and benchmarks. *J. Chem. Phys.*, **130**, 054104.
- 383 Lee, C., Yang, W. T., & Parr, R. G. (1988). Development of the colle-salvetti correlation-energy formula into a functional of the electron density. *Phys. Rev. B*, **37**, 785-789.
- 384 Martin, J. M. L., & Taylor, P. R. (1997). Accurate *ab initio* quartic force field for *trans*-hnnh and treatment of resonance polyads. *Spectrochim. Acta A*, **53**, 1039-1050.
- 385 McCall, B. J. (2006). Dissociative recombination of cold h₃⁺ and its interstellar implications. *Phil. Trans. Royal Soc. A*, **364**, 2953-2963.
- 386 McCarthy, M. C., Gottlieb, C. A., & Cernicharo, J. (2019). Building blocks of dust: A coordinated laboratory and astronomical study of the archetype AGB carbon star IRC+10216. *J. Molec. Spectrosc.*, **356**, 7-20.
- 387 Mehner, T., Göckes, H. J., Schunck, S., & Schnöckel, H. (1980). Dimeres SiO₂ matrix-ir-untersuchungen und ab initio scf-rechnungen. *Z. Anorg. Allg. Chem.*, **580**, 121-130.
- 388 Mills, I. M. (1972). Vibration-rotation structure in asymmetric- and symmetric-top molecules. In K. N. Rao & C. W. Mathews (Eds.), *Molecular spectroscopy - modern research* (p. 115-140). New York: Academic Press.
- 389 Molster, F. J., Lim, T. L., Sylvester, R. J., Waters, L. B. F. M., Barlow, M. J., Beintema, D. A., ... Schmitt, B. (2001). The complete iso spectrum of ngc 6302. *Astron. Astrophys.*, **372**, 165-172.
- 390 Palmer, C. Z., & Fortenberry, R. C. (2018). Rovibrational considerations for the monomers and dimers of magnesium hydride (MgH₂) and magnesium fluoride

- 426 (MgF₂). *J. Phys. Chem. A*, *122*, 7079-7088.
- 427 Papousek, D., & Aliev, M. R. (1982). *Molecular vibration-rotation spectra*. Amsterdam: Elsevier.
- 428 Prascher, B. P., Woon, D. E., Peterson, K. A., Dunning, T. H., & Wilson, A. K.
- 429 (2011). Gaussian basis sets for use in correlated molecular calculations. vii. valence, core-valence, and scalar relativistic basis sets for Li, Be, Na, and Mg.
- 430 *Theor. Chem. Acc.*, *128*, 69-82.
- 431 Raghavachari, K., Trucks, G. W., Pople, J. A., & Head-Gordon, M. (1989). A fifth-
- 432 order perturbation comparison of electron correlation theories. *Chem. Phys.*
- 433 *Lett.*, *157*, 479-483.
- 434 Rho, J., Gomez, H. L., Boogert, A., Smith, M. W. L., Lagage, P.-O., Dowell, D., ...
- 435 Cami, J. (2018). A dust twin of Cas A: Cool dust and 21 μm silicate dust
- 436 feature in the supernova remnant G54.1+0.3. *Mon. Not. Royal Astron. Soc.*,
- 437 *479*, 5101-5123.
- 438 Rouillé, G., Jäger, C., Krasnokutski, S. A., Krebszb, M., & Henning, T. (2014). Cold
- 439 condensation of dust in the ISM. *Farad. Discuss.*, *168*, 449-460.
- 440 Savage, B. D., & Sembach, K. R. (1996). Interstellar abundances from absorption-
- 441 line observations with the *Hubble Space Telescope*. *Annu. Rev. Astron. Astro-*
- 442 *phys.*, *34*, 279-329.
- 443 Schnöckel, H. (1978). Ir spectroscopic detection of molecular SiO₂. *Angew. Chem.*
- 444 *Int. Ed. Engl.*, *17*, 616-617.
- 445 Schnöckel, V. H. (1980). Matrixreaktionen von SiO. ir-spektroskopischer nachweis
- 446 der molekeln SiO₂ und OSiCl₂. *Z. Anorg. Allg. Chem.*, *460*, 37-50.
- 447 Shavitt, I., & Bartlett, R. J. (2009). *Many-body methods in chemistry and physics:*
- 448 *Mbpt and coupled-cluster theory*. Cambridge: Cambridge University Press.
- 449 Stephan, C. J., & Fortenberry, R. C. (2017). The interstellar formation and spectra
- 450 of the noble gas, proton-bound HeHHe⁺, HeHNe⁺ and HeHAr⁺ complexes.
- 451 *Mon. Not. Royal Astron. Soc.*, *469*, 339-346.
- 452 Tremblay, B., Roy, P., Manceron, L., Alikhani, M. E., & Roy, D. (1996). Vibrational
- 453 spectrum and structure of silicon trioxide SiO₃: A matrix isolation infrared
- 454 and density functional theory study. *J. Chem. Phys.*, *104*, 2773-2781.
- 455 Valencia, E. M., Worth, C. J., & Fortenberry, R. C. (2020). Enstatite (MgSiO₃) and
- 456 forsterite (Mg₂SiO₄) monomers and dimers: Highly-detectable infrared and
- 457 radioastronomical molecular building blocks. *Mon. Not. Royal Astron. Soc.*,
- 458 *492*, 276-282.
- 459 Wang, L.-S., Desai, S. R., Wu, H., & Nicholas, J. B. (1997). Small silicon oxide clus-
- 460 ters: Chains and rings. *Z. Phys. D*, *40*, 36-39.
- 461 Wang, L.-S., Wu, H., Desai, S. R., Fan, J., & Colson, S. D. (1996). A photoelectron
- 462 spectroscopic study of small silicon oxide clusters: SiO₂, Si₂O₃, and Si₂O₄. *J.*
- 463 *Phys. Chem.*, *100*, 8697-8700.
- 464 Watson, J. K. G. (1977). Aspects of quartic and sextic centrifugal effects on ro-
- 465 tational energy levels. In J. R. During (Ed.), *Vibrational spectra and structure*
- 466 (p. 1-89). Amsterdam: Elsevier.
- 467 Werner, H.-J., Knowles, P. J., Knizia, G., Manby, F. R., & Schütz, M. (2012). Mol-
- 468 pro: A General-Purpose Quantum Chemistry Program Package. *WIREs Com-*
- 469 *put. Mol. Sci.*, *2*, 242–253.
- 470 Werner, H.-J., Knowles, P. J., Knizia, G., Manby, F. R., Schütz, M., Celani, P., ...
- 471 Wang, M. (2015). *Molpro, version 2015.1, a package of ab initio programs*.
- 472 Cardiff, UK. (see <http://www.molpro.net>)
- 473 Westbrook, B. R., & Fortenberry, R. C. (2020). Anharmonic frequencies of (MO)₂
- 474 and related hydrides for M = Mg, Al, Si, P, S, Ca, & Ti and heuristics for
- 475 predicting anharmonic corrections of inorganic oxides. *J. Phys. Chem. A*
- 476 (*submitted*)
- 477 White, W. M. (2013). *Geochemistry* (1st ed.). Hoboken, NJ: Wiley.

- 480 Wilson, R. W., Penzias, A. A., Jefferts, K. B., Kutner, M., & Thaddeus, P. (1971).
481 Discovery of interstellar silicon monoxide. *Astrophys. J.*, *167*, L97-L100.
482 Yang, W. T., Parr, R. G., & Lee, C. T. (1986). Various functionals for the kinetic
483 energy density of an atom or molecule. *Phys. Rev. A*, *34*, 4586-4590.
484 Yu, Q., Bowman, J. M., Fortenberry, R. C., Mancini, J. S., Lee, T. J., Crawford,
485 T. D., ... Francisco, J. S. (2015). The structure, anharmonic vibrational fre-
486 quencies, and intensities of NNHNN⁺. *J. Phys. Chem. A*, *119*, 11623-11631.
487 Zhao, D., Doney, K. D., & Linnartz, H. (2014). Laboratory gas-phase detection of
488 the cyclopropenyl cation (*c*-C₃H₃⁺). *Astrophys. J. Lett.*, *791*, L28.

1 **Supplemental Information for “Spectral**
 2 **Characterization for Small Clusters of Silicon and**
 3 **Oxygen: SiO₂, SiO₃, Si₂O₃, & Si₂O₄”**

4 **Mason B. Gardner¹, Brent R. Westbrook¹, and Ryan C. Fortenberry¹**

5 ¹Department of Chemistry & Biochemistry, University of Mississippi, University, MS 38677-1848

6 **Introduction**

7 The explicit CCSD(T)-F12b/cc-pVTZ-F12 force constants for each of the molecules
 8 explored. They are given in units of mdyne/(Åⁿ·rad^m) numbered from the symmetry-
 9 internal coordinates given in the text.

Table S1. CCSD(T)-F12b/cc-pVTZ-F12 force constants for SiO₂

4	4	0	0	0.423766259855
3	3	0	0	0.423766211032
2	2	0	0	9.112568406691
1	1	0	0	9.280510189762
4	4	1	0	-0.561596903890
3	3	1	0	-0.561596082870
2	2	1	0	-38.726137784528
1	1	1	0	-39.471154081588
4	4	4	4	0.359773378775
4	4	3	3	0.683611533991
3	3	3	3	0.361891002070
4	4	2	2	-0.804604628590
3	3	2	2	-0.803545817450
2	2	2	2	136.514960010751
4	4	1	1	0.027162155485
3	3	1	1	0.028407813978
2	2	1	1	135.90959842323
1	1	1	1	137.129507870339

Table S2. CCSD(T)-F12b/cc-pVTZ-F12 force constants for SiO₃

1	1	0	0	9.593251755369	3	2	2	2	-10.841399942476
2	1	0	0	0.020317264205	3	3	1	1	-0.928709892230
2	2	0	0	6.175872995167	3	3	2	1	0.709080890870
3	1	0	0	0.027966975167	3	3	2	2	36.402882897569
3	2	0	0	-1.879514109745	3	3	3	1	0.489792625850
3	3	0	0	6.154725332648	3	3	3	2	-150.627489211387
4	4	0	0	5.400667716233	3	3	3	3	748.599740366254
5	4	0	0	0.060071158680	4	4	1	1	0.044880119037
5	5	0	0	0.338878981838	4	4	2	1	0.216627388092
6	6	0	0	0.500633887434	4	4	2	2	77.105244430278
1	1	1	0	-56.875124864289	4	4	3	1	1.058300987324
2	1	1	0	-0.286271769474	4	4	3	2	12.268129236786
2	2	1	0	-0.061126772121	4	4	3	3	-43.701877754418
2	2	2	0	-24.448452284040	4	4	4	4	78.487904596218
3	1	1	0	-0.249791618390	5	4	1	1	0.0000908224868
3	2	1	0	-0.1661115607672	5	4	2	1	-0.056241596139
3	2	2	0	6.455600817448	5	4	2	2	-0.168252544859
3	3	1	0	-0.341875325469	5	4	3	1	0.200987409404
3	3	2	0	-21.780762781098	5	4	3	2	-0.043598136539
3	3	3	0	80.965619208057	5	4	3	3	-0.871788790145
4	4	1	0	-0.247019715133	5	4	4	4	0.897134819534
4	4	2	0	-22.141561198732	5	5	1	1	-0.092708702622
4	4	3	0	-2.083042459491	5	5	2	1	0.220987201935
5	4	1	0	-0.115963170075	5	5	2	2	0.008959291030
5	4	2	0	0.010349296600	5	5	3	1	0.166719095925
5	4	3	0	-0.324048573980	5	5	3	2	-0.042676575777
5	5	1	0	-0.344488100188	5	5	3	3	-0.144496289900
5	5	2	0	-0.165531828561	5	5	4	4	-0.281554039784
5	5	3	0	-0.096202691644	5	5	5	4	0.089697331009
6	6	1	0	-0.436942519454	5	5	5	5	0.237161089921
6	6	2	0	-4.626097373435	6	6	1	1	-1.133182657608
6	6	3	0	14.379198844142	6	6	2	1	-0.172767409510
1	1	1	1	279.489567735293	6	6	2	2	14.834754840529
2	1	1	1	-0.003138098573	6	6	3	1	-0.781460413976
2	2	1	1	0.159693594846	6	6	3	2	-57.037475106406
2	2	2	1	-0.269591553292	6	6	3	3	231.184327712308
2	2	2	2	79.322436459600	6	6	4	4	-4.600652854360
3	1	1	1	-0.265877807624	6	6	5	4	-0.421052504480
3	2	1	1	0.336226531556	6	6	5	5	2.021540456128
3	2	2	1	0.094799152526	6	6	6	6	98.159664984538

Table S4. CCSD(T)-F12b/cc-pVTZ-F12 force constants for Si₂O₄

12	12	0	0	1.5052177	6	6	1	0	-10.8955301
11	11	0	0	3.4380046	5	5	1	0	-0.1769573
11	10	0	0	1.6085544	5	4	1	0	-0.1344538
10	10	0	0	1.4861017	4	4	1	0	-13.2745196
9	9	0	0	4.7880909	3	3	1	0	-0.2114673
9	8	0	0	0.2305831	3	2	1	0	0.0426781
8	8	0	0	9.5984462	2	2	1	0	-2.4634107
7	7	0	0	0.4874767	3	1	1	0	-0.1104480
7	6	0	0	-0.0153111	2	1	1	0	0.3392645
6	6	0	0	4.4563956	1	1	1	0	-13.5017494
5	5	0	0	0.3862562	12	12	12	12	-60.5367835
5	4	0	0	0.3156321	12	12	11	11	-5.2442897
4	4	0	0	3.1459507	11	11	11	11	16.9170223
3	3	0	0	9.6515276	12	12	11	10	-12.0536259
3	2	0	0	-0.0367923	11	11	11	10	-4.3405671
2	2	0	0	2.5458314	12	12	10	10	-26.9068233
3	1	0	0	0.0198368	11	11	10	10	-3.0261947
2	1	0	0	-0.2676806	11	10	10	10	-6.7489281
1	1	0	0	4.9711604	10	10	10	10	-13.8197903
12	11	9	0	-1.0666611	12	12	9	9	-0.4256177
12	10	9	0	-0.3821905	11	11	9	9	-17.3925953
12	11	8	0	-1.8473227	11	10	9	9	0.6057806
12	10	8	0	-1.9713577	10	10	9	9	-0.5366798
12	12	3	0	-1.8895568	9	9	9	9	12.4008141
11	11	3	0	-1.7806184	12	12	9	8	0.4400029
11	10	3	0	-1.7734222	11	11	9	8	1.2760603
10	10	3	0	-1.7677520	11	10	9	8	0.9857538
9	9	3	0	-0.5732631	10	10	9	8	0.3291087
9	8	3	0	-0.3637721	9	9	9	8	0.7429297
8	8	3	0	-40.2930191	12	12	8	8	1.2515269
7	7	3	0	-0.3695357	11	11	8	8	-0.2294819
7	6	3	0	-0.0931883	11	10	8	8	0.9048638
6	6	3	0	-0.0080361	10	10	8	8	1.4965264
5	5	3	0	-0.2740490	9	9	8	8	0.1401472
5	4	3	0	-0.2180328	9	8	8	8	-0.1735030
4	4	3	0	-0.2760485	8	8	8	8	140.1888729
3	3	3	0	-40.3875189	12	11	9	7	-0.0366224
12	12	2	0	-0.5724076	12	10	9	7	0.0021799
11	11	2	0	0.1741417	12	11	8	7	0.0209271
11	10	2	0	0.2190144	12	10	8	7	0.0344425
10	10	2	0	-0.5099257	12	12	7	7	0.5598222
9	9	2	0	1.7294489	11	11	7	7	1.4604507
9	8	2	0	0.1170418	11	10	7	7	1.9644730
8	8	2	0	0.0312180	10	10	7	7	1.7362410
7	7	2	0	0.1757038	9	9	7	7	0.2997647
7	6	2	0	0.0986588	9	8	7	7	0.2535532
6	6	2	0	-0.4822610	8	8	7	7	-0.1066505
5	5	2	0	0.1242985	7	7	7	7	0.2006736
5	4	2	0	0.1166824	12	11	9	6	-0.0379303
4	4	2	0	0.7144730	12	10	9	6	-0.0021799
3	3	2	0	0.0705488	12	11	8	6	-0.0034878
3	2	2	0	-0.0955508	12	10	8	6	0.0170032
2	2	2	0	0.1699830	12	12	7	6	-0.9139685
12	12	1	0	0.0622657	11	11	7	6	-1.1572764
11	11	1	0	5.5537311	11	10	7	6	-0.2733603
11	10	1	0	-0.3252612	10	10	7	6	-0.0699389
10	10	1	0	-0.0309021	9	9	7	6	0.3680479
9	9	1	0	-11.7737133	9	8	7	6	0.1953196
9	8	1	0	-0.2848449	8	8	7	6	0.1212824
8	8	1	0	-0.1776558	7	7	7	6	0.1756657
7	7	1	0	-0.1778230	12	12	6	6	-1.3918542
7	6	1	0	-0.0917942	11	11	6	6	-20.7202227

Table S5. CCSD(T)-F12b/cc-pVTZ-F12 force constants for Si₂O₄ contd.

11	10	6	6	-1.0847806	7	7	3	3	-0.0495594	10	10	2	1	0.1199264
10	10	6	6	-0.7618291	7	6	3	3	0.1069137	9	9	2	1	-1.1132032
9	9	6	6	22.8318894	6	6	3	3	-0.0445515	9	8	2	1	-0.1822402
9	8	6	6	-0.1671688	5	5	3	3	0.0117510	8	8	2	1	0.1123403
8	8	6	6	-0.0105761	5	4	3	3	0.0489730	7	7	2	1	-0.1596248
7	7	6	6	-0.1256472	4	4	3	3	0.0624784	7	6	2	1	0.0422901
7	6	6	6	-0.0035225	3	3	3	3	139.9007595	6	6	2	1	-0.6736468
6	6	6	6	8.4062955	12	11	9	2	-0.2737962	5	5	2	1	-0.1547418
12	11	9	5	-0.0095915	12	10	9	2	0.4346734	5	4	2	1	-0.5768033
12	10	9	5	0.0130794	12	11	8	2	-0.1630570	4	4	2	1	-0.8850106
12	11	8	5	-0.0265948	12	10	8	2	0.6975701	3	3	2	1	0.0429104
12	10	8	5	-0.0217990	12	12	3	2	0.7942119	3	2	2	1	-0.0489036
12	12	5	5	1.1787742	11	11	3	2	-0.7329291	2	2	2	1	-1.5685296
11	11	5	5	1.3014890	11	10	3	2	-0.1704687	12	12	1	1	-0.4674084
11	10	5	5	1.7212389	10	10	3	2	0.7097331	11	11	1	1	-14.8873326
10	10	5	5	1.7070058	9	9	3	2	-0.3591187	11	10	1	1	-0.1126219
9	9	5	5	0.1282888	9	8	3	2	-0.1286145	10	10	1	1	-0.3973593
9	8	5	5	0.2611828	8	8	3	2	0.2124528	9	9	1	1	26.4259966
8	8	5	5	0.0371393	7	7	3	2	-0.0707606	9	8	1	1	0.1957724
7	7	5	5	0.2099587	7	6	3	2	-0.1177149	8	8	1	1	0.0225191
7	6	5	5	0.2263975	6	6	3	2	0.1049398	7	7	1	1	0.0108889
6	6	5	5	-0.0715429	5	5	3	2	-0.2044325	7	6	1	1	0.0867209
5	5	5	5	0.2269462	5	4	3	2	-0.8846061	6	6	1	1	25.0526085
12	11	9	4	0.0187471	4	4	3	2	-0.0984891	5	5	1	1	0.1028190
12	10	9	4	0.0148233	3	3	3	2	0.1909926	5	4	1	1	0.5953724
12	11	8	4	0.0418542	12	12	2	2	-0.1244722	4	4	1	1	35.9583554
12	10	8	4	-0.0122074	11	11	2	2	-1.6415210	3	3	1	1	0.0621003
12	12	5	4	1.5234718	11	10	2	2	-0.7655843	3	2	1	1	0.0698978
11	11	5	4	0.4546069	10	10	2	2	-0.2286635	2	2	1	1	2.5511729
11	10	5	4	0.7215491	9	9	2	2	-2.5925774	3	1	1	1	-0.0718655
10	10	5	4	1.1744121	9	8	2	2	0.1984342	2	1	1	1	-0.0444305
9	9	5	4	0.3825392	8	8	2	2	-0.1801460	1	1	1	1	30.6720701
9	8	5	4	0.2097070	7	7	2	2	0.0566748					
8	8	5	4	0.0878158	7	6	2	2	0.2737798					
7	7	5	4	0.2131604	6	6	2	2	-4.2422336					
7	6	5	4	0.0222350	5	5	2	2	0.0153139					
6	6	5	4	-0.0305531	5	4	2	2	0.1479179					
5	5	5	4	0.2803003	4	4	2	2	-5.5748232					
12	12	4	4	-0.1449868	3	3	2	2	-0.1857288					
11	11	4	4	-21.2976080	3	2	2	2	0.0399136					
11	10	4	4	0.8828468	2	2	2	2	6.2780710					
10	10	4	4	0.3297905	12	11	9	1	0.2057832					
9	9	4	4	31.6385350	12	10	9	1	-0.0326986					
9	8	4	4	0.3666903	12	11	8	1	0.3016991					
8	8	4	4	0.1059420	12	10	8	1	0.0034878					
7	7	4	4	-0.0075751	12	12	3	1	-0.0565573					
7	6	4	4	0.1832354	11	11	3	1	0.2790852					
6	6	4	4	30.5400374	11	10	3	1	0.3147785					
5	5	4	4	0.0852797	10	10	3	1	-0.0618522					
5	4	4	4	0.3448255	9	9	3	1	0.4928468					
4	4	4	4	54.9654774	9	8	3	1	0.2663846					
12	11	9	3	0.8113613	8	8	3	1	-0.0176873					
12	10	9	3	0.0928640	7	7	3	1	0.1346881					
12	11	8	3	0.5327692	7	6	3	1	0.1312303					
12	10	8	3	1.0223763	6	6	3	1	-0.1373641					
12	12	3	3	0.5912478	5	5	3	1	0.2713247					
11	11	3	3	-0.2043077	5	4	3	1	0.8671669					
11	10	3	3	0.5730161	4	4	3	1	0.2756845					
10	10	3	3	0.7799912	3	3	3	1	-0.0098185					
9	9	3	3	0.0537292	12	12	2	1	-0.0301654					
9	8	3	3	-0.2179968	11	11	2	1	0.3182979					
8	8	3	3	139.9578700	11	10	2	1	-0.0174392					